

Ni Nanoparticles Inlaid Nickel Phyllosilicate as a Metal–Acid Bifunctional Catalyst for Low-Temperature Hydrogenolysis Reactions

Xiao Kong,^{†,‡,⊥} Yifeng Zhu,^{†,‡,⊥} Hongyan Zheng,[§] Xianqing Li,[§] Yulei Zhu,^{*,†,§} and Yong-Wang Li^{†,§}

[†]State Key Laboratory of Coal Conversion, Institute of Coal Chemistry, Chinese Academy of Sciences, Taiyuan 030001, P.R. China

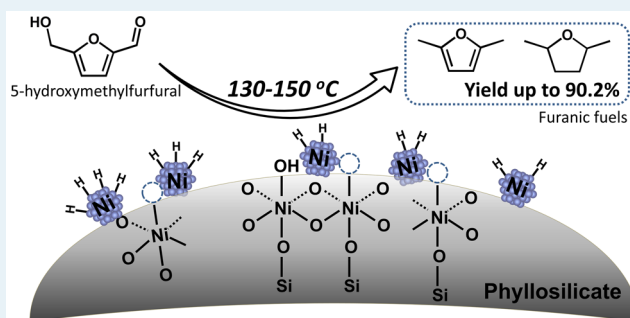
[‡]University of Chinese Academy of Sciences, Beijing 100049, P.R. China

[§]Synfuels China Co. Ltd, Beijing, 101407, P.R. China

Supporting Information

ABSTRACT: Hydrogenolysis of carbon–oxygen bonds is a versatile synthetic method, of which hydrogenolysis of bioderived 5-hydroxymethylfurfural (HMF) to furanic fuels is especially attractive. However, low-temperature hydrogenolysis (in particular over non-noble catalysts) is challenging. Herein, nickel nanoparticles (NPs) inlaid nickel phyllosilicate (NiSi-PS) are presented for efficient hydrogenolysis of HMF to yield furanic fuels at 130–150 °C, being much superior with impregnated Ni/SiO₂ catalysts prepared from the same starting materials. NiSi-PS also shows a 2-fold HMF conversion intrinsic rate and 3-fold hydrogenolysis rate compared with the impregnated Ni/SiO₂. The superior performance originated from the synergy of highly dispersed nickel NPs and substantially formed acid sites due to coordinatively unsaturated Ni (II) sites located at the remnant nickel phyllosilicate structure, as revealed by detailed characterizations. The model reactions over the other reference catalysts further highlighted the metal–acid synergy for hydrogenolysis reactions. NiSi-PS can also efficiently catalyze low-temperature hydrogenolysis of bioderived furfural and 5-methylfurfural, demonstrating a great potential for other hydrogenolysis reactions.

KEYWORDS: hydrogenolysis, heterogeneous catalysis, nickel, silica, 5-hydroxymethylfurfural

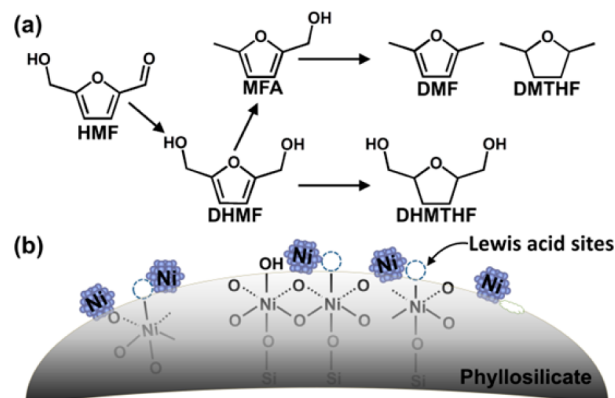


1. INTRODUCTION

Silica-supported metal NPs are widely employed solid catalysts for sustainable synthesis of fuels and chemicals. However, SiO₂ is always considered as an inert oxide, suffering from the weak binding and dispersing ability for metal NPs.¹ The resulted SiO₂ supported catalysts therefore commonly have low reactivity. Moreover, it has hardly any surface acidity, making it a nonpreferred choice for reactions needing acid functionality, such as hydrogenolysis of carbon–oxygen bonds.²

Hydrogenolysis of carbon–oxygen bonds (e.g., aldehydes, ethers, esters, and CO_x) is an important method for producing chemicals with lower oxygen contents.^{2b,3} A typical and promising case is hydrogenolysis of bioderived HMF to furanic fuels (e.g., 2,5-dimethylfuran (DMF) and 2,5-dimethyltetrahydrofuran (DMTHF)) (Scheme 1 and Table S1).^{3a,4} This reaction is generally catalyzed by noble metals (e.g., Ru, Pt, and Pd) at high temperatures (180–220 °C),^{3a,5} which leaves ample room for improvements. Low-temperature hydrogenolysis is charming because it is more energy saving and produces minimized humins and/or C–C cracking byproducts. Reported works on low-temperature hydrogenolysis of HMF to furanic fuels are relatively scarce. A Pd/Zn/C was reported to catalyze HMF hydrogenolysis with a yield of 85% at 150 °C.⁶ A Ru/Co₃O₄ catalyst could give a yield of 93.4% at 130 °C for

Scheme 1. (a) Reaction Route of HMF Hydrogenolysis to Furanic Fuels. (b) Ni-Based Catalyst with Protogenetic Metal–Acid Bifunctionality Derived from Nickel Phyllosilicate



Received: May 22, 2015

Revised: August 2, 2015

Published: August 27, 2015

this reaction.⁷ Rauchfuss et al. proposed that Pd/C catalyst combined with formic acid solvent could enable an efficient synthesis of DMF from fructose at 120–150 °C.⁸ It seems that usage of noble metals and/or a specific solvent is a prerequisite for low-temperature hydrogenolysis. Low-temperature hydrogenolysis of HMF to furanic fuels using non-noble catalysts has never been reported.

Among the non-noble catalysts, nickel-based catalysts attract great interest in the conversion of lignocellulosic biomass, especially in lignin-derived model compounds.^{3b,9} Grilc et al.^{9a,b} reported a series of Ni-based bifunctional catalysts (ML-77(Ni), NiMo/Al₂O₃) for efficient hydrodeoxygenation of solvolysed lignocellulosic biomass. The group of Lercher reported a Ni/HZSM-5 catalyst for hydrodeoxygenation of pyrolysis oil to hydrocarbons under moderate conditions.^{3b,10} In contrast, HMF hydrogenation over Ni-based catalysts was scarcely investigated. Fu et al.¹¹ reported that a bifunctional Ni–W₂C/AC catalyst is effective for DMF synthesis at 180 °C. Recently, we have also shown that nickel-based catalysts (Raney Ni and Ni–Al₂O₃ derived from hydrotalcite) are promising candidates for HMF hydrogenolysis at high temperatures.¹² Nevertheless, it is particularly encouraging to convert HMF under mild conditions over Ni-based catalysts.

Yet, hydrogenation of C=C bonds to yield 2,5-dihydroxymethyltetrahydrofuran (DHMTHF) dominates at low temperatures over Ni catalysts (Scheme 1).^{12a} The formed DHMTHF was rather stable and could not be easily converted, which are detrimental for production of furanic fuels.^{11,12b,13}

The efficient synthesis of furanic fuels relies on the fast conversion of C–O to C=C bonds under mild conditions, and the development of bifunctional metal–acid catalyst is a prerequisite. Herein, we present a nickel NPs inlaid nickel phyllosilicate (NiSi-PS) catalyst which featured with highly dispersed nickel NPs and large amounts of proximal acid sites for HMF hydrogenolysis. The catalyst displays excellent hydrogenolysis ability at low temperatures (130–150 °C), which cannot be achieved over supported Ni/SiO₂ catalysts. The metal–acid synergy over NiSi-PS promotes the intrinsic activity for both HMF conversion and hydrogenolysis reactions (turnover frequency (TOF), 1404 and 1487 h⁻¹ respectively), in comparison with Ni/SiO₂ catalyst (703 and 479 h⁻¹). NiSi-PS can also efficiently catalyze hydrogenolysis of bioderived furfural and 5-methylfurfural at low temperatures.

2. RESULTS AND DISCUSSION

2.1. Formation of Nickel Phyllosilicate.

Nickel phyllosilicate (tetrahedral/octahedral sheet = 2:1, theoretical Ni loading is 36 wt %) is a sandwich-like structure with a formula of Ni₃Si₄O₁₂H₂ (Figure S1). Two sheets of tetrahedral SiO₄ sandwich the octahedral Ni²⁺ species, which are coordinated to six O atoms or OH groups.¹⁴ The material is composed of fragments of the same layer-like structure, which has large proportions of edges. An illustration for the dynamic color changes of suspensions during ammonia evaporation is shown in Figure S1. With the formation of nickel phyllosilicate, the dark-blue solution of precursors changed gradually into a light-green suspension. The impregnated Ni/SiO₂ reference with same Ni loadings of 36 wt % (denoted as NiSi-IMP-36) was prepared with the same starting materials. The impregnation method is typically fit for low Ni loading. Therefore, Ni/SiO₂ catalyst with Ni loading of 20 wt % (denoted as NiSi-IMP-20) was also prepared as a reference.

The formation of nickel phyllosilicate can be proved by FT-IR (Figure 1), XRD (Figure 2a), and TEM (Figure 2b). The

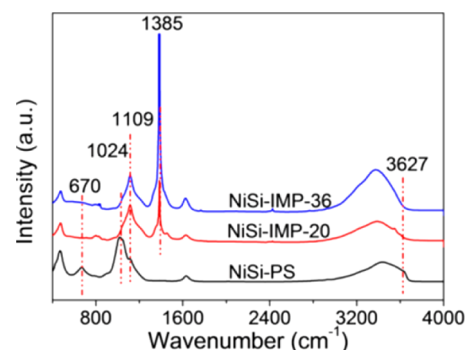


Figure 1. FT-IR spectra of different precursors.

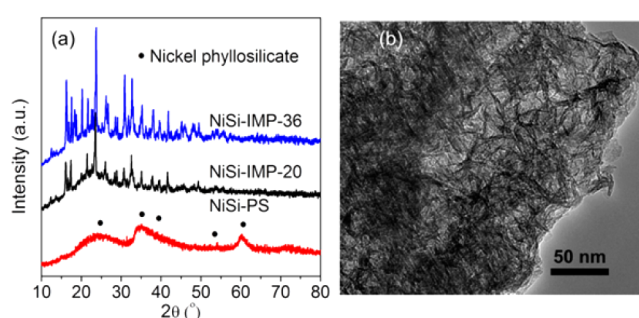


Figure 2. (a) XRD patterns of precursors and (b) TEM image of NiSi-PS precursor.

bands at 670, 1024, and 3627 cm⁻¹ are attributed to δ_{OH} vibration, symmetric in-plane Si–O vibration, and ν_{OH} stretching of nickel phyllosilicate (Figure 1).¹⁵ No related bands assigned to phyllosilicate were detected for NiSi-IMP-36 and NiSi-IMP-20 precursors, whereas the bands at 1109 and 1385 cm⁻¹ were observed, which were attributed to amorphous SiO₂ and NO₃²⁻ respectively.¹⁶ The presence of nickel nitrates was confirmed by XRD peaks (Figure 2a). Broad XRD peaks at 26.7°, 33.7°, 39.7°, 53.2°, and 60.9° of NiSi-PS precursor can be attributed to nickel phyllosilicate (PDF#43-0664) (Figure 2a). The characteristic “fibrous” microstructures also confirmed the presence of phyllosilicate over NiSi-PS precursor (Figure 2b).^{14a} The above results revealed that nickel phyllosilicate was achieved via ammonia evaporation, which would substantially change the properties of resulted catalysts.

2.2. Characterization of Resulted Catalysts.

The precursors were calcined at 600 °C. Ni loadings of all catalysts were in line with the nominal values (Table 1). The N₂ adsorption–desorption isotherms of the calcined samples are shown in Figure S2. All catalysts displayed a type IV isotherms shape. NiSi-IMP-20 and NiSi-IMP-36 catalysts exhibited a typical H1 hysteresis behavior, whereas the shape of the hysteresis loop in NiSi-PS was a superposition of types H1 and H3. This is because of the formation of fibrous nickel phyllosilicate over the NiSi-PS catalyst.^{14a,17} The fibrous structure also promotes the increase of BET surface area and pore volume (Table 1). Calcined NiSi-PS exhibited higher surface area and pore volume than the impregnated catalysts due to the existence of layered structures.

Figure 3a shows the FT-IR spectra of calcined catalysts. The characteristic bands at 670, 1024, and 3627 cm⁻¹ indicated the

Table 1. Physicochemical Properties of Catalysts

catalyst	loading (wt %) ^a	S _{BET} (m ² /g) ^b	V _p (cm ³ /g) ^b	d _p (nm) ^b	d _{Ni} (nm) ^c	S _{Ni} (mmol/g) ^d	S _{acid} (μmol NH ₃ /g) ^e
SiO ₂	-	153.9	0.19	4.7	-	-	-
NiSi-PS	36.1	352.5	0.76	7.0	3.3	0.19	1.84
NiSi-IMP-20	19.8	142.3	0.23	5.4	15.7	0.10	0.43
NiSi-IMP-36	34.5	98.7	0.17	5.4	35.1	0.02	0.31

^aNi loadings were determined by ICP experiments. ^bThe BET surface area, pore volume, and pore diameter were determined by N₂ physical adsorption. ^cThe sizes of Ni were calculated by Ni (200) reflection ($2\theta = 43.3^\circ$) based on the Scherrer equation for impregnated samples and calculated by HRTEM for NiSi-PS catalyst. ^dS_{Ni} was calculated on the basis of H₂-TPD results. ^eS_{acid} was calculated on the basis of NH₃-TPD results.

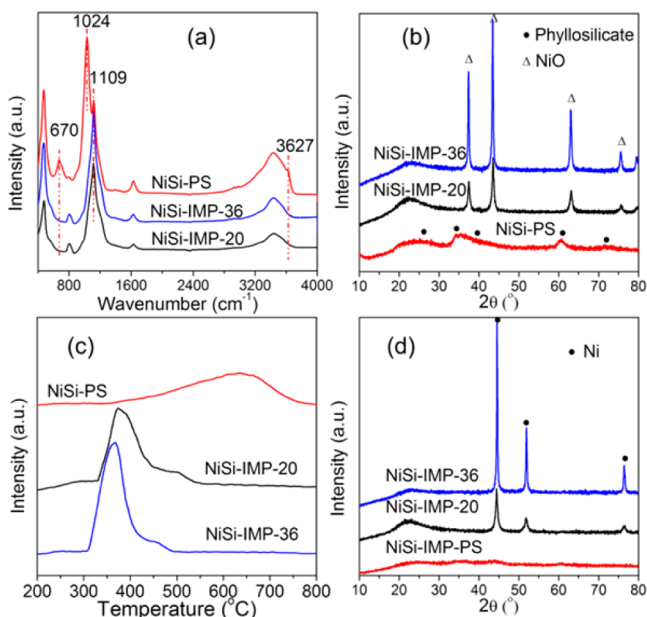


Figure 3. (a) FT-IR patterns of calcined catalysts, (b) XRD patterns of calcined catalysts, (c) TPR results of calcined catalysts, (d) XRD patterns of reduced catalysts.

preservation of nickel phyllosilicate after calcination of NiSi-PS precursor, as also evidenced by XRD pattern (Figure 3b). For NiSi-IMP-36 and NiSi-IMP-20, the disappearance of the band at 1385 cm⁻¹ indicated decomposition of nickel nitrates. XRD results showed the formation of large crystalline NiO particles. The broad XRD peak around 22° is the feature of amorphous SiO₂. The above results showed that calcined NiSi-PS consisted of nickel phyllosilicate, whereas impregnated catalysts were composed of large crystalline NiO and amorphous SiO₂.

TPR results can reveal the reduction behavior of Ni²⁺ species (Figure 3c). NiSi-IMP-36 and NiSi-IMP-20 catalysts both exhibited a reduction peak at 350–450 °C and a shoulder around 500 °C, which were ascribed to the reduction of bulk NiO and Ni²⁺ ions interacting with SiO₂ respectively. NiSi-PS showed a broad peak with higher temperatures, which could be assigned to reduction of Ni²⁺ located in nickel phyllosilicate.¹⁸ The retarded reduction process of Ni species could retain the phyllosilicate structure partially.

The catalysts were reduced at 500 °C under H₂ atmosphere for 2 h. XRD results suggested that NiSi-IMP-20 and NiSi-IMP-36 catalysts were totally reduced (Figure 3d). The Ni particle sizes of NiSi-IMP-20 and NiSi-IMP-36 were 15.7 and 35.1 nm, respectively (Table 1). In contrast, no evident XRD peaks related to metallic Ni were detected for reduced NiSi-PS, indicating that the metallic Ni particles were too small to be detected by XRD. We thus performed HRTEM to determine the distribution of metallic Ni (Figure 4). The corresponding

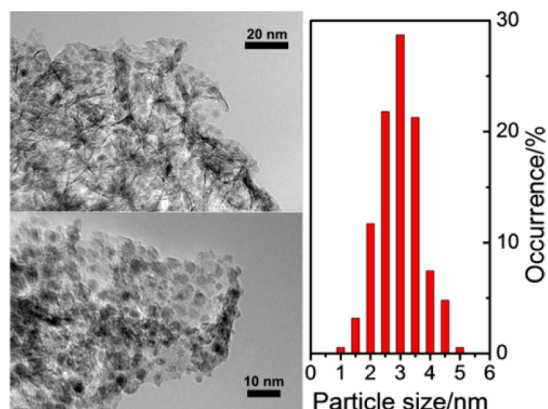


Figure 4. HRTEM images and particle size distribution histogram of reduced NiSi-PS.

size distribution histogram showed that NiSi-PS exhibited a small size of 3.3 nm (Figure 4 and Table 1). Thus, highly dispersed Ni NPs were formed upon reduction of nickel phyllosilicate. As evidenced by HRTEM images, the “fibrous” structure still existed upon reduction. The results indicated the remnant of nickel phyllosilicate, which was consistent with TPR results. The unreduced nickel phyllosilicate could act as an additional host for Ni⁰ NPs, which would exhibit different properties with support SiO₂ (Figure 5a). Besides, Ni NPs and phyllosilicate were closely contacted, facilitating the binding

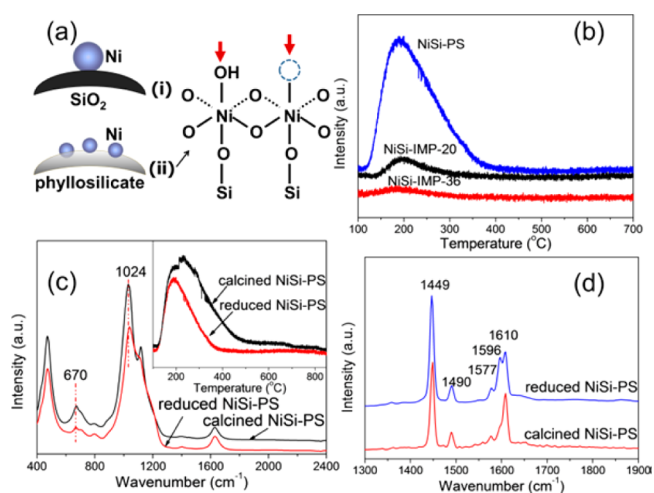
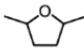
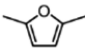
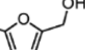
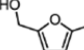
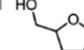


Figure 5. Characterizations of surface acidity. (a) Schematic representation of reduced impregnated Ni/SiO₂ catalysts, NiSi-PS and origin of surface acidity. (b) NH₃-TPD results of reduced catalysts, (c) FT-IR and NH₃-TPD results of calcined and reduced NiSi-PS catalysts, and (d) Py-IR spectra of calcined and reduced NiSi-PS catalysts.

Table 2. Catalytic Performance of Catalysts for HMF Hydrogenolysis to Furanic Fuels^a

Entry	Catalyst	Amount (g)	T (°C)	Time (h)	Conv. (%)	Sel. (%)					Others ^b
											
1	NiSi-PS	0.08	150	3	100	26.1	64.1	0	0	9.2	0.6
2	NiSi-IMP-36	0.08	150	3	41.5	0	11.4	16.7	61.0	9.0	1.9
3	NiSi-IMP-20	0.08	150	3	50.9	0	18.5	17.8	53.0	9.7	1.0
4	NiSi-IMP-20	0.08	150	20	100	9.4	14.4	0	0	50.2	26.0
5	NiSi-IMP-20	0.08	180	3	78.4	2.7	32.6	23.3	33.5	6.9	1.0
6	NiSi-PS	0.08	130	3	100	0	68.0	18.0	0	11.1	2.9
7	NiSi-PS	0.08	130	6	100	9.8	69.1	5.4	0	13.5	2.2
8	NiSi-PS	0.15	130	3	100	10.5	72.9	0	0	13.7	2.9

^aHMF 1.5 g, 1.5 MPa, 1,4-dioxane 38 mL. ^bOthers mainly include furfuryl alcohol and 5-methyltetrahydrofurfuryl alcohol.

and dispersion of Ni NPs. H₂-TPD results showed that NiSi-PS had a surface metallic Ni concentration of 0.19 mmol/g (Table 1), which was greatly higher than impregnated references.

Surface acidity of the reduced catalysts was studied by NH₃-TPD (Figure 5b). The peaks around 200 °C were observed for all the catalysts, corresponding to the weak acid sites. The impregnated catalysts displayed small NH₃ desorption peak area due to the slight acidity of SiO₂ support. In contrast, NiSi-PS exhibited a large NH₃ desorption peak area, indicating the significant amounts of acid sites. The amounts of acid sites were determined through NH₃-TPD results and shown in Table 1. To address the origin of acidity, FT-IR and NH₃-TPD of calcined and reduced NiSi-PS were compared. Upon reduction, the intensities of peaks at 670 and 1024 cm⁻¹ decreased (Figure 5c). The results indicated that phyllosilicate was partially destroyed after reduction due to the release of Ni⁰. The partial destruction caused a decrease of acid concentration (inset of Figure 5c), indicating that surface acidity of NiSi-PS was associated with phyllosilicate structure. The acid sites could stem from two distinct locations of phyllosilicate: coordinatively unsaturated (cus) Ni(II) sites near the edges/surfaces of phyllosilicate and surface OH groups (Figure 5a). The former are Lewis acid centers, whereas the latter may acquire proton donor (Brønsted acid) and hydrogen bond (H-bond) donor properties.

The nature of acid sites is determined by the pyridine adsorbed IR (Py-IR) spectra (Figure 5d). The strong bands at 1449, 1610 and a small band at 1490 cm⁻¹ are consistent with pyridine adsorbed on Lewis acid sites.¹⁹ Our data supported that the acidity was mainly arisen from cus-Ni(II) sites located in the remnant phyllosilicate structure. The cus-Ni(II) sites are formed due to the broken bonds near the edges/surfaces of phyllosilicate.²⁰ The absence of a band at 1540 cm⁻¹ ruled out Brønsted acidity caused by surface OH groups. The bands at 1577 and 1596 cm⁻¹ were observed, which are assigned to vibration of pyridine interacting with OH groups via H-bonds.¹⁹ Previous work by Lercher et al.^{3b} on C–O cleavage of substituted phenols shows that the presence of proximal acid sites increases the activities of catalyst by a synergistic action. Similarly, the substantially generated acid sites of NiSi-PS could cooperate with highly dispersed Ni sites and benefit for HMF hydrogenolysis.

2.3. Catalytic Behavior. Furanic fuels (DMF and DMTHF) can be obtained via tandem hydrogenolysis of

HMF passing through 2,5-dihydroxymethylfuran (DHMF) and 5-methylfurfuryl alcohol (MFA) intermediates (Scheme 1). To our knowledge, the low-temperature hydrogenolysis has never been reported over non-noble catalysts. Table 2 shows performances of the three catalysts for furanic fuel production. At 150 °C, NiSi-PS exhibited a conversion of 100% and a high yield of furanic fuels (DMF and DMTHF, 90.2%) within 3 h, revealing the high activity toward HMF hydrogenolysis (entry 1). NiSi-IMP-20 showed a HMF conversion of 50.9%, whereas NiSi-IMP-36 gave a conversion of 41.5% (entry 2, 3). Both catalysts showed low selectivity toward furanic fuels. The major byproducts are MFA and DHMF, indicating the insufficient reactivity of impregnated Ni/SiO₂ catalysts. One important reason could be the low amounts of Ni sites, as revealed by H₂-TPD (Table 1). However, with prolonging reaction time to 20 h (entry 4), the hydrogenolysis products (DMF and DMTHF) were not promoted selectively over NiSi-IMP-20 catalyst, despite of the complete conversion of HMF. Instead, large amounts of DHMTHF (50.2%) were obtained, revealing that total hydrogenation of HMF dominates over the impregnated catalyst at 150 °C. The hydrogenolysis reaction can be promoted only at high temperature (180 °C, entry 5), which was consistent with previous reports.^{12a} The results indicated that although important, the high dispersion cannot account alone for the superiority of NiSi-PS compared to impregnated Ni/SiO₂ catalysts.

At 130 °C, a furanic fuel yield of 68.0% was received over NiSi-PS within 3 h (entry 6). The yield can be improved to 78.9% when the reaction time was prolonged to 6 h (entry 7). High yield of furanic fuels (83.4%) can also be realized after increasing the catalyst dosage from 0.08 to 0.15 g (entry 8). Combined with the above characterizations, the results revealed that the synergy effects of Ni and acid sites over NiSi-PS are responsible for the superior reactivity. Besides, DHMTHF selectivity over NiSi-PS increased slightly at 130 °C compared with that at 150 °C, due to the favorable hydrogenation of HMF to DHMTHF at lower temperature.

The NiSi-PS catalyst was also compared with impregnated Ni/Al₂O₃ (20 wt %), Ni/ZrO₂ (20 wt %) and commercial Raney Ni catalysts (Table S2). Among the reference catalysts, Ni/Al₂O₃ showed the highest selectivity of furanic fuels (38.0%), which was still lower than that for NiSi-PS. Raney Ni exhibited high selectivity for DHMTHF, demonstrating the high reactivity toward C=C hydrogenation and low reactivity

for C–O hydrogenolysis. High selectivity of furanic fuels can be achieved over Ni/Al₂O₃ upon prolonging the reaction time. The characterization results revealed that Ni/Al₂O₃ has similar acid concentration with NiSi-PS (Figure S3) and lower dispersion of Ni species than that of NiSi-PS (Figure S4). The comparisons hence further highlighted the synergy between metal and acid sites for C–O hydrogenolysis. Further optimizations of metal–acid sites over NiSi-PS catalyst are needed.

NiSi-IMP-20 was chosen as reference to further elucidate the effect of acid sites over NiSi-PS. The catalytic behavior of NiSi-PS and NiSi-IMP-20 under low conversions was compared (Figure 6). To obtain the intrinsic activity of catalysts, the yield

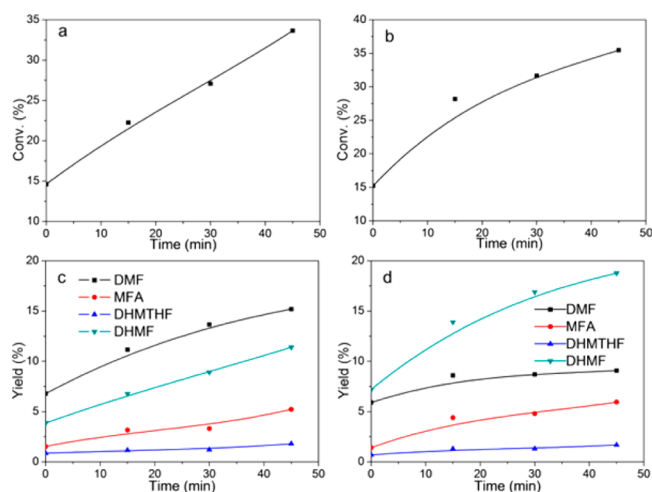


Figure 6. HMF hydrogenation on NiSi-PS (a, c) and NiSi-IMP-20 (b, d) catalyst as a function of reaction time. Reaction conditions: 1.5 g of HMF, 38 mL of 1,4-dioxane, 150 °C, 1.5 MPa H₂. NiSi-PS 0.02 g, NiSi-IMP-20 0.08 g.

of furanic fuels was lower than 20%. Thus, during the investigated reaction time, MFA and DHMF increased monotonously. Most importantly, the catalysts exhibited different product distributions at similar conversions (Figure 6c,d). NiSi-PS exhibited higher DMF yield, whereas NiSi-IMP-20 showed a higher DHMF yield. For example, at a HMF conversion of ~35%, the yield of DMF to DHMF over NiSi-PS was 1.33; however, the ratio was only 0.48 for NiSi-IMP-20, indicating the stronger hydrogenolysis ability of NiSi-PS catalyst. TOFs based on numbers of Ni sites were calculated for HMF conversion (TOF_{HMF}) and hydrogenolysis of C–O bonds (TOF_{C–O}), respectively (see Supporting Information for details). About 2-fold TOF_{HMF} was obtained over NiSi-PS, in compared with NiSi-IMP-20 (Table 3). Moreover, the attained TOF_{C–O} value of NiSi-PS catalyst was 1487 h⁻¹, which was

Table 3. Parameters in the Hydrogenolysis of HMF under Low Conversions

catalyst	DMF/DHMF ^a	TOF _{HMF} (h ⁻¹) ^b	TOF _{C–O} (h ⁻¹) ^c	TOF _{C–O} / TOF _{HMF}
NiSi-PS	1.33	1404	1487	1.1
NiSi-IMP-20	0.48	703	479	0.7

^aThe ratio of yield of DMF to DHMF. ^bCalculated on the basis of converted HMF. ^cCalculated on the basis of DMF, DMTHF, and MFA products.

about 3 times that of NiSi-IMP-20 catalyst. Finally, TOF_{C–O}/TOF_{HMF} was larger over NiSi-PS as compared with that of NiSi-IMP-20, demonstrating that the hydrogenolysis step could be promoted more significantly by the synergy of highly dispersed Ni sites and acid sites over NiSi-PS.

NiSi-PS catalyst was also compared to previously reported catalysts especially that operated under mild conditions, including Pd/Zn/C,⁶ Ru/Co₃O₄,⁷ Pd/C with formic acid⁸ (Table S2). The NiSi-PS, with the moderate HMF/active metal ratio (52.0), can give similar fuel yields, which was comparable to the reported noble metal catalysts. In all, we report an efficient catalytic system for low-temperature hydrogenolysis of HMF to furanic fuels without usage of noble metals and specific solvents. Design of an efficient Ni catalyst with lower loadings is also an important direction.

In terms of the different properties of DMF and DMTHF as fuels (Table S1), the time course for tunable production of DMF and DMTHF was tested (Figure 7). DMF yield increased

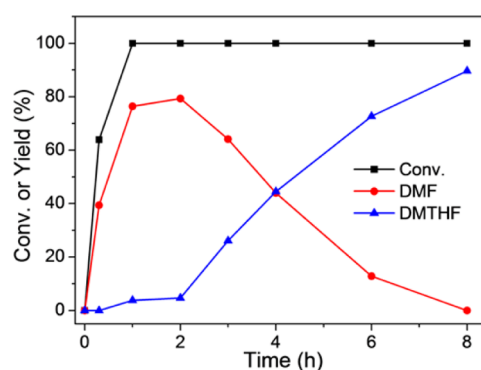


Figure 7. Conversion and yield of DMF/DMTHF over NiSi-PS versus reaction time. Reaction conditions: 1.5 g of HMF, 38 mL of 1,4-dioxane, 0.08 g of NiSi-PS, 150 °C, 1.5 MPa H₂.

first and reached the maximum at 2 h (~79.3%). Further increase of reaction time resulted in the conversion of DMF to DMTHF. Finally, a high yield of DMTHF (89.7%) was achieved over NiSi-PS catalyst. These results demonstrated the synthesis of furanic fuels with tunable properties.

On the basis of the catalytic results and the reported works,²¹ we proposed the possible mechanism for HMF hydrogenolysis over NiSi-PS catalyst. The initial hydrogenation of HMF to DHMF occurred over metallic Ni sites which have strong C=O hydrogenation ability. Lewis acid, presenting in the preserved nickel phyllosilicate can facilitate polarization and activation of C–O bonds of DHMF and MFA. Thus, DMF/DMTHF can be produced through the synergy of Ni and proximal acid sites.^{12b} DMF/DMTHF can also be generated by direct cleavage of C=O bonds. The C=O bonds of HMF might be adsorbed onto the surface via an η²(C,O) configuration. The C atom is bonded to a metallic Ni site, and the O atom is bonded to acid sites. The formed CH₂OH-(C₄H₃O)–CH= intermediate was then hydrogenated into furanic fuels.²² In all, compared with other references, NiSi-PS catalyst provides the required proximity of metallic and acid sites and catalyzes the hydrogenolysis of HMF effectively.

NiSi-PS was extended to hydrogenolysis of 5-methylfurfural and furfural (Table 4) which were generally performed at high temperatures (e.g., 180 °C).^{5c,23} The catalyst gave a conversion of 100% and high selectivities toward hydrogenolysis products at 150 °C. For example, 2-methylfuran (2-MF) and 2-

Table 4. Hydrogenolysis of Bioderived Chemicals over the NiSi-PS Catalyst^a

feedstock	conv. (%)	products (sel. (%))
5-methylfurfural	100	DMF (15.7), DMTHF (76.9)
furfural	100	2-MF (0), 2-MTHF (78.3), THFA (17.4)

^a1.5 MPa, 150 °C, 3 h, feedstock 1.5 g, catalyst 0.08 g 1,4-dioxane 38 mL.

methyltetrahydrofuran (2-MTHF) were obtained with a total yield of 78.3% from furfural. The major byproduct was tetrahydrofurfuryl alcohol (THFA). The results showed the great potential of NiSi-PS for low-temperature hydrogenolysis reactions.

3. CONCLUSION

We have reported that nickel nanoparticles (NPs) inlaid nickel phyllosilicate (NiSi-PS) catalyst could effectively catalyze hydrogenolysis of HMF to yield furanic fuels at low temperatures (130–150 °C), whereas supported Ni/SiO₂ catalyst only shows weak hydrogenolysis ability. At 150 °C, the overall yield of furanic fuels can be up to 90.2% within 3 h, whereas the yield could also be around 83.4% at 130 °C. In particular, NiSi-PS shows a higher HMF conversion intrinsic rate (1404 h⁻¹) and hydrogenolysis rate (1487 h⁻¹) in comparison with supported Ni/SiO₂ (703 h⁻¹ and 479 h⁻¹, respectively). We have clarified that synergy of highly dispersed nickel NPs and substantially formed acid sites due to coordinatively unsaturated Ni (II) sites located at remnant nickel phyllosilicate structure mainly contributes to the realization of low-temperature hydrogenolysis. In addition, the NiSi-PS demonstrated a great potential for low-temperature hydrogenolysis of furfural and 5-methylfurfural. The attractive features of NiSi-PS might be also promising for hydrogenolysis of lignin-derived model compounds, providing guiding principles for future catalyst design for biomass conversion.

4. EXPERIMENTAL SECTION

4.1. Chemicals. The following materials have been used for the preparation of catalysts: nickel(II) nitrate hexahydrate (Sinopharm. Co. Ltd.), silica sol (Qingdao Ocean Chemical Co., Ltd.), and ammonia aqueous solution (Sinopharm. Co. Ltd.). 5-Hydroxymethylfurfural was purchased from Shanghai De-Mo Pharmaceutical Science and Technology Co. Ltd. 1,4-Dioxane was purchased from Sinopharm. Co. Ltd. 5-Methylfurfural was purchased from T.C.I. These chemicals were used without further purification. Furfural was used after distillation.

4.2. Catalyst Preparation. NiSi-PS catalyst was prepared by a modified ammonia evaporation procedure.^{14a} A certain amount of Ni(NO₃)₂·6H₂O and a 25 wt % ammonia aqueous solution dissolved in water were mixed and stirred for 15 min. Silica sol (40 wt %) was then added to the solution and stirred for 12 h at room temperature. Then the suspension was heated in a water bath preheated to 80 °C to evaporate ammonia until the pH value of the suspension decreased to 6–7. Then the precipitate was filtered, washed with distilled water, and then dried at 80 °C for 12 h. A green material was received and calcined at 600 °C in air. For detailed comparison, two supported Ni/SiO₂ catalysts were prepared by impregnation method with a Ni loading of 36 and 20 wt % respectively. The support SiO₂ for impregnation was obtained by drying silica sol gel at 80 °C. The catalysts were denoted as NiSi-IMP-36 and

NiSi-IMP-20. The reference Ni/Al₂O₃ and Ni/ZrO₂ catalysts were also prepared by impregnated method with Ni loadings of 20 wt %.

4.3. Evaluation. The tests were performed in a 100 mL tank reactor. Prior to the test, the catalysts were reduced in a quartz tube under H₂ flow at 500 °C for 2 h. The reduced catalysts were then protected by 1,4-dioxane and transferred to the reactor. For a typical procedure based on our previous works,¹² the reactor was fed with HMF (1.5 g), 1,4-dioxane (38 mL), and a certain amount of prerduced catalyst and then sealed and purged by H₂ (5 times). After that, the reactor was filled with 1.5 MPa H₂ and heated to the desired temperature. The timing was then started at the moment the temperature reached the desired value. After the test, the reactor was quenched in ice-water, and then the liquid and gas products were analyzed by a GC instrument with a FID detector and a capillary column (J&W DB-WAX). The conversion and selectivity were determined by calibrated area normalization.

4.4. Catalyst Characterization. The catalysts were characterized by inductively coupled plasma-mass spectrometry (ICP), N₂ physical adsorption, X-ray diffraction (XRD), high-resolution transmission electron microscope (HRTEM), infrared spectra (IR), pyridine adsorbed IR (Py-IR), temperature-programmed reduction (TPR), H₂ temperature-programmed desorption (H₂-TPD), and NH₃ temperature-programmed desorption (NH₃-TPD). More details could be found in Supporting Information.

■ ASSOCIATED CONTENT

Supporting Information

The Supporting Information is available free of charge on the ACS Publications website at DOI: 10.1021/acscatal.5b01080.

Experimental details, Table S1 to S3, Figure S1 to S4 (PDF)

■ AUTHOR INFORMATION

Corresponding Author

*(Y. Zhu) E-mail: zhuyulei@sxicc.ac.cn. Tel.: +86 351 7117097. Fax: +86 351 7560668.

Author Contributions

[†]These authors contributed equally (X.K. and Y.Z.).

Notes

The authors declare no competing financial interest.

■ ACKNOWLEDGMENTS

We thank Dr. G. Ding for helpful suggestions. This project was supported by the Major State Basic Research Development Program of China (No. 2012CB215305).

■ REFERENCES

- (1) Kennedy, G.; Baker, L. R.; Somorjai, G. A. *Angew. Chem.* **2014**, *126*, 3473–3476.
- (2) (a) Vasiliadou, E. S.; Heracleous, E.; Vasalos, I. A.; Lemonidou, A. A. *Appl. Catal., B* **2009**, *92*, 90–99. (b) Zhu, Y.; Kong, X.; Cao, D.-B.; Cui, J.; Zhu, Y.; Li, Y.-W. *ACS Catal.* **2014**, *4*, 3675–3681.
- (3) (a) Román-Leshkov, Y.; Barrett, C. J.; Liu, Z. Y.; Dumesic, J. A. *Nature* **2007**, *447*, 982–985. (b) Song, W.; Liu, Y.; Baráth, E.; Zhao, C.; Lercher, J. A. *Green Chem.* **2015**, *17*, 1204–1218. (c) Serrano-Ruiz, J. C.; Dumesic, J. A. *Energy Environ. Sci.* **2011**, *4*, 83–99. (d) Chheda, J. N.; Huber, G. W.; Dumesic, J. A. *Angew. Chem., Int. Ed.* **2007**, *46*, 7164–7183.

- (4) (a) Grochowski, M. R.; Yang, W.; Sen, A. *Chem. - Eur. J.* **2012**, *18*, 12363–12371. (b) Chidambaram, M.; Bell, A. T. *Green Chem.* **2010**, *12*, 1253–1262.
- (5) (a) Wang, G.-H.; Hilgert, J.; Richter, F. H.; Wang, F.; Bongard, H.-J.; Spliethoff, B.; Weidenthaler, C.; Schüth, F. *Nat. Mater.* **2014**, *13*, 293–300. (b) Jae, J.; Zheng, W. Q.; Lobo, R. F.; Vlachos, D. G. *ChemSusChem* **2013**, *6*, 1158–1162. (c) Scholz, D.; Aellig, C.; Hermans, I. *ChemSusChem* **2014**, *7*, 268–275.
- (6) Saha, B.; Bohn, C. M.; Abu-Omar, M. M. *ChemSusChem* **2014**, *7*, 3095–3101.
- (7) Zu, Y.; Yang, P.; Wang, J.; Liu, X.; Ren, J.; Lu, G.; Wang, Y. *Appl. Catal., B* **2014**, *146*, 244–248.
- (8) Thananathanachon, T.; Rauchfuss, T. B. *Angew. Chem.* **2010**, *122*, 6766–6768.
- (9) (a) Celic, T. B.; Grilc, M.; Likozar, B.; Tusar, N. N. *ChemSusChem* **2015**, *8*, 1703–1710. (b) Grilc, M.; Likozar, B.; Levec, J. *Appl. Catal., B* **2014**, *150–151*, 275–287. (c) Sergeev, A. G.; Hartwig, J. F. *Science* **2011**, *332*, 439–443. (d) Sergeev, A. G.; Webb, J. D.; Hartwig, J. F. *J. Am. Chem. Soc.* **2012**, *134*, 20226–20229. (e) Grilc, M.; Likozar, B.; Levec, J. *Biomass Bioenergy* **2014**, *63*, 300–312.
- (10) Zhao, C.; Lercher, J. A. *Angew. Chem.* **2012**, *124*, 6037–6042.
- (11) Huang, Y. B.; Chen, M. Y.; Yan, L.; Guo, Q. X.; Fu, Y. *ChemSusChem* **2014**, *7*, 1068–1072.
- (12) (a) Kong, X.; Zhu, Y.; Zheng, H.; Dong, F.; Zhu, Y.; Li, Y.-W. *RSC Adv.* **2014**, *4*, 60467–60472. (b) Kong, X.; Zheng, R.; Zhu, Y.; Ding, G.; Zhu, Y.; Li, Y.-W. *Green Chem.* **2015**, *17*, 2504–2514.
- (13) Chen, J.; Liu, R.; Guo, Y.; Chen, L.; Gao, H. *ACS Catal.* **2015**, *5*, 722–733.
- (14) (a) Zhang, C.; Yue, H.; Huang, Z.; Li, S.; Wu, G.; Ma, X.; Gong, J. *ACS Sustainable Chem. Eng.* **2012**, *1*, 161–173. (b) Burattin, P.; Che, M.; Louis, C. *J. Phys. Chem. B* **1998**, *102*, 2722–2732.
- (15) Kermarec, M.; Carriat, J. Y.; Burattin, P.; Che, M.; Decarreau, A. *J. Phys. Chem.* **1994**, *98*, 12008–12017.
- (16) Cavani, F.; Trifirò, F.; Vaccari, A. *Catal. Today* **1991**, *11*, 173–301.
- (17) (a) Chen, L.; Guo, P.; Qiao, M.; Yan, S.; Li, H.; Shen, W.; Xu, H.; Fan, K. *J. Catal.* **2008**, *257*, 172–180. (b) Yue, H.; Zhao, Y.; Zhao, S.; Wang, B.; Ma, X.; Gong, J. *Nat. Commun.* **2013**, *4*, 2339–2346.
- (18) Zhang, C.; Zhu, W.; Li, S.; Wu, G.; Ma, X.; Wang, X.; Gong, J. *Chem. Commun.* **2013**, *49*, 9383–9385.
- (19) Zaki, M. I.; Hasan, M. A.; Al-Sagheer, F. A.; Pasupulety, L. *Colloids Surf., A* **2001**, *190*, 261–274.
- (20) (a) Peri, J. *Discuss. Faraday Soc.* **1966**, *41*, 121–134. (b) Giese, R.; Costanzo, P.; Van Oss, C. *Phys. Chem. Miner.* **1991**, *17*, 611–616. (c) Shirai, M.; Aoki, K.; Torii, K.; Arai, M. *Appl. Catal., A* **1999**, *187*, 141–146. (d) Arai, M.; Kanno, M.; Nishiyama, Y.; Torii, K.; Shirai, M. *J. Catal.* **1999**, *182*, 507–510.
- (21) (a) Panagiotopoulou, P.; Martin, N.; Vlachos, D. G. *ChemSusChem* **2015**, *8*, 2046–2054. (b) Gilkey, M. J.; Panagiotopoulou, P.; Mironenko, A. V.; Jenness, G. R.; Vlachos, D. G.; Xu, B. *ACS Catal.* **2015**, *5*, 3988–3994.
- (22) Shi, D.; Vohs, J. M. *ACS Catal.* **2015**, *5*, 2177–2183.
- (23) (a) Stevens, J. G.; Bourne, R. A.; Twigg, M. V.; Poliakoff, M. *Angew. Chem., Int. Ed.* **2010**, *49*, 8856–8859. (b) Sitthisa, S.; An, W.; Resasco, D. E. *J. Catal.* **2011**, *284*, 90–101.